

## **EUV Spectral Purity Filter for Full IR-to-VUV Out-of-Band Rejection, With Out-of-Band Power Recycling**

Kenneth C. Johnson kjinovation@earthlink.net 3/6/2018

### Abstract

A plasma light source for EUV lithography can be spectrally filtered by a phase-Fresnel collector mirror to reject all out-of-band (OoB) radiation in the IR-to-VUV spectral range, leaving only pure EUV in the filtered output. EUV collection efficiency is not significantly compromised, and EUV conversion efficiency can be enhanced by recycling rejected or uncollected OoB radiation back to the plasma via retroreflection. [U.S. Patent 9,612,370.]

### Introduction

A phase-Fresnel optic is a grating-type surface (reflecting or transmitting) with a sawtooth profile similar to a Fresnel lens, which preserves optical phase coherence between Fresnel facets at a particular “blaze” wavelength. [Ref. 1] This paper discusses the application of phase-Fresnel spectral filters for extreme ultraviolet (EUV) lithography using a laser-produced plasma (LLP) source, which requires elimination or separation of the infrared (IR) drive-laser radiation from the EUV. Ideally, the full OoB spectrum from the deep IR to the vacuum ultraviolet (VUV) should be eliminated in the EUV collection optics. [Ref’s. 2, 3]

One type of filter that has been developed for lithography is an LPP collection mirror with a lamellar (rectangular-section) diffraction grating on its surface, which is designed to extinguish the zero-order IR radiation at the 10.6-  $\mu\text{m}$  laser wavelength. [Ref’s. 4-8] The IR radiation is scattered into first and higher diffraction orders, and an aperture at the collector’s intermediate focus (IF) blocks the scattered IR while transmitting the focused EUV radiation beam. The EUV beam is substantially unaffected by the grating because its wavelength (13.5 nm) is much smaller than the grating period (which is of order 1 mm). In a variation of this process, one of the grating’s first diffraction orders in the IR is directed back (“recycled”) to the plasma source to improve conversion efficiency. [Ref. 9]

A limitation of spectral filtering via diffractive IR scattering is that it only eliminates OoB radiation at one or very few design wavelengths. Also, power recycling is limited by the grating diffraction efficiency.

An alternative LPP filtering mechanism discussed in this paper similarly rejects IR by diverting it into a ring or halo around the IF aperture, but not via diffractive scattering. Instead, the collection mirror shape is configured to reflect the specularly reflected radiation away from the focus, and a blazed phase-Fresnel grating on the mirror surface selectively diffracts the 13.5-nm EUV toward the focus. The grating dimensions are too small to significantly affect most OoB radiation, and complete OoB rejection can be achieved over the full IR-to-VUV spectral range by taking advantage of the grating’s chromatic dispersion properties. Moreover, efficient power recycling can be achieved by retroreflecting the rejected OoB radiation (or radiation that does not intercept the collector) back to the plasma.

## EUV Spectral Filtering Mechanisms

Kierey et al. [Ref. 10] demonstrated a grazing-incidence, phase-Fresnel mirror that spatially separates EUV and OoB radiation, as illustrated in Figure 1. The grating is located in the convergent beam of an EUV collector, near the intermediate focus (IF). The first diffracted order in the EUV is focused onto the IF, while the zero-order OoB radiation is directed outside of the IF aperture. (The EUV reflection efficiency is 59%.) The mirror comprises sawtooth-profile grating lines in ruthenium (shown schematically in cross-section in Figure 1), which are illustrated perpendicular to the incidence plane although the lines could alternatively be oriented parallel to the incidence plane. The grating design could be considerably improved by employing modern fabrication technology (e.g., to allow a nonuniform distribution of grating blaze angles).

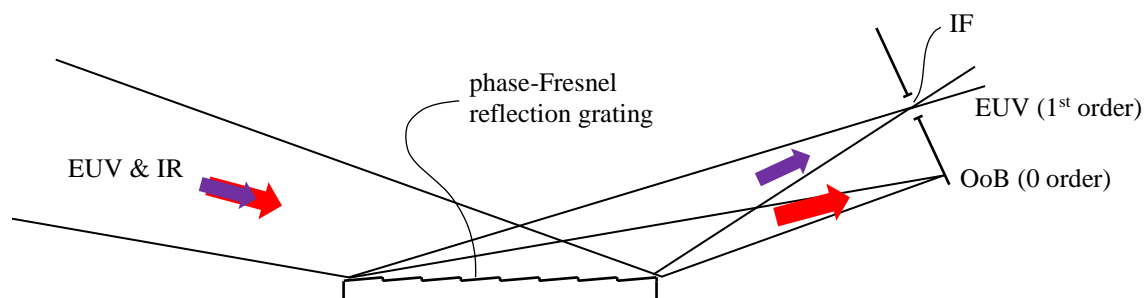


Figure 1. A phase-Fresnel, grazing-incidence reflection grating in ruthenium separates the 1<sup>st</sup>-order EUV (13.5 nm) from the 0-order OoB (10.6  $\mu\text{m}$ ).

Phase-Fresnel EUV reflection gratings operating at near-normal incidence have been researched by Liddle et al. [Ref. 11] and by Boogaard et al. (2009) [Ref. 12], although it is unclear from these publications how such gratings might be incorporated into an LPP collector for spectral filtering.

EUV/OoB separation could alternatively be achieved by a free-standing transmission phase-Fresnel grating, similar to transmission filters described by Chkhalo et al. [Ref. 13] and Suzuki et al. [Ref. 14]. These filters employ OoB -reflecting/EUV-transmitting films, but similar structures could employ phase-Fresnel transmission gratings to separate the EUV and OoB as illustrated in Figure 2. (The grating can be formed in a molybdenum layer.) The transmission grating is functionally similar to the reflection grating of Figure 1.

A preferred method of spectral filtering is to incorporate the filtering function in the EUV collector's main condenser mirror, rather than in a separate optical element. The mirror's reflective coatings can be designed to reflect EUV and suppress IR, but EUV efficiency is compromised relative to a conventional coating. [Ref. 15] An alternative approach, which circumvents this limitation, is to reject IR via diffractive scattering from a grating-type filtering mechanism as illustrated in Figure 3. [Ref's. 4-8]

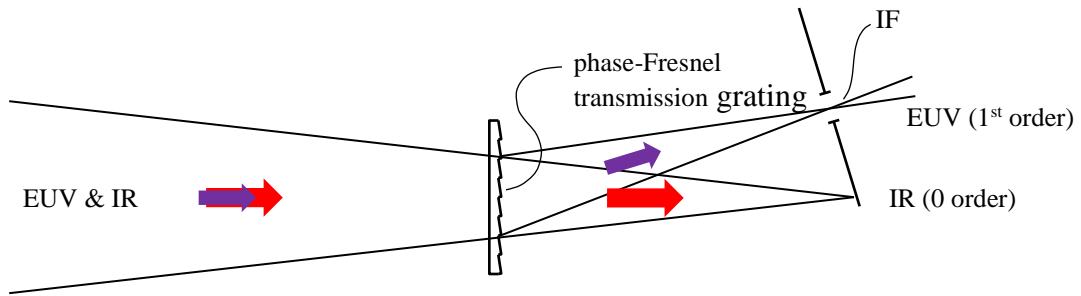


Figure 2. A phase-Fresnel, transmission grating (e.g. in molybdenum) separates the 1<sup>st</sup>-order EUV (13.5 nm) from the 0-order OoB.

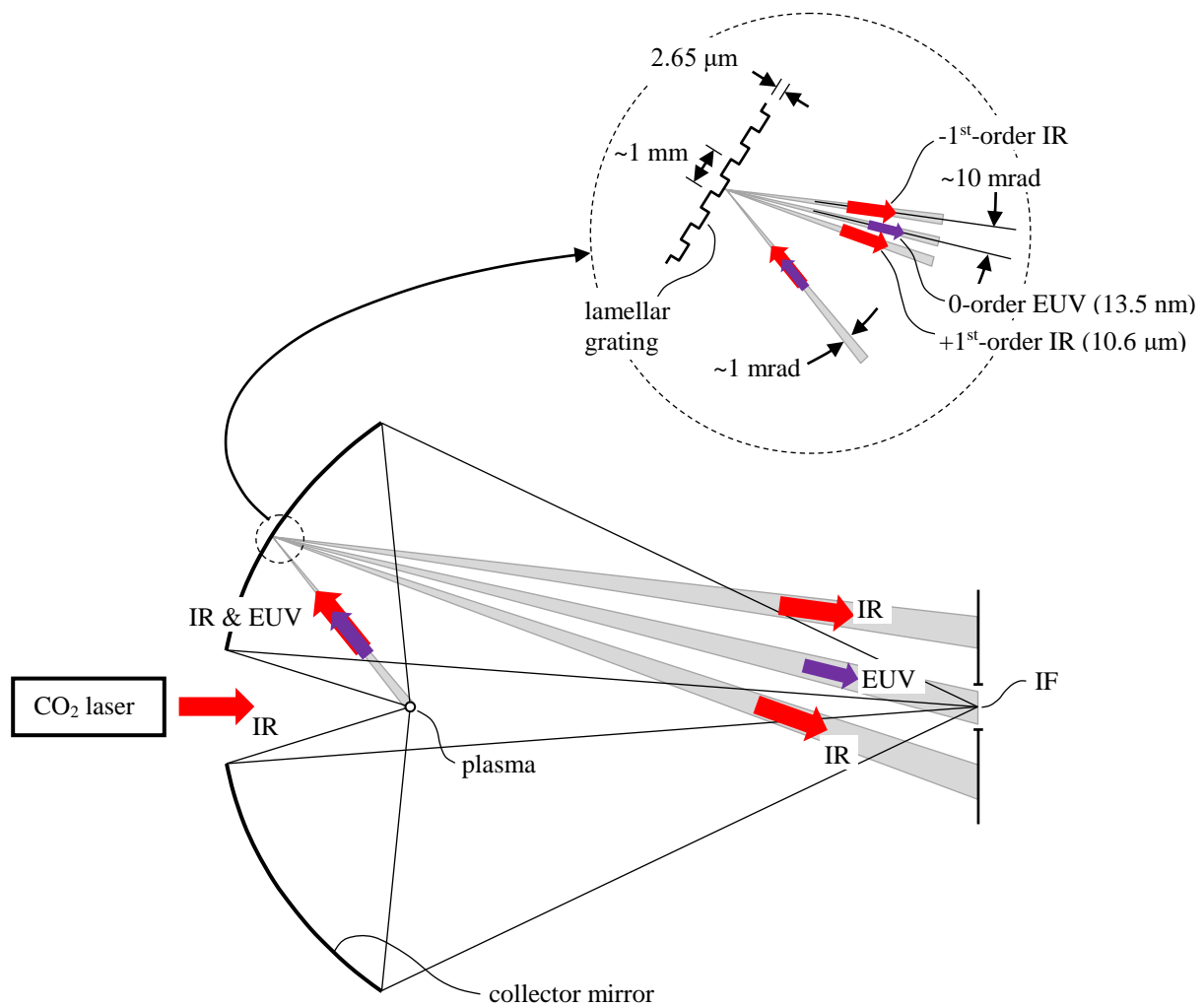


Figure 3. Lamellar-grating spectral filter.

The diffractive filter is a lamellar (rectangular-profile) diffraction grating with annular grating zones formed on the mirror surface. (A cross section of the grating is shown in the enlarged detail view of Figure 3.) In contrast to the grating structures illustrated in Figures 1 and 2, the Figure 3 structure operates to diffract IR radiation while having minimal impact on the EUV beam. The grating scatters the IR into a halo around the IF aperture through which the EUV transmits.

As illustrated in the detail view in Figure 3, the grating depth is approximately  $2.65\ \mu\text{m}$  (one-quarter of the  $\text{CO}_2$  drive laser's IR wavelength of  $10.6\ \mu\text{m}$ ), resulting in extinction of the zero diffraction order and redirection of IR radiation into first and higher orders. The grating period is of order 1 mm, resulting in a first-order scattering angle of approximately  $(10.6\ \mu\text{m})/(1\ \text{mm})$ , or roughly 10 mrad. By comparison, the plasma source's subtend angle at the grating is typically of order 1 mrad (e.g., for a 200- $\mu\text{m}$  plasma diameter and 200-mm condenser focal length). All of the light cones illustrated in Figure 3 have approximately 1 mrad extent, so the 10 mrad IR scatter angle is more than sufficient to separate the first-order IR and zero-order EUV light cones. The grating also induces some diffractive scatter in the EUV, but the scatter angle is only of order  $(13.5\ \text{nm})/(1\ \text{mm})$ , i.e.  $13.5\ \mu\text{rad}$ , which is insignificant in relation to the plasma's 1 mrad angular extent.

In a variation of this approach, the grating is designed to direct one of the first diffraction orders in the IR back onto the plasma to improve the EUV conversion efficiency. [Ref. 9] About 37% of the collected IR power at the 10.6- $\mu\text{m}$  laser wavelength can be recycled by this method, but it would require a much smaller grating period to retroreflect the IR. For example, to retroreflect the first diffraction order with a  $30^\circ$  incidence angle, the grating period would be equal to the 10.6- $\mu\text{m}$  IR wavelength. Deposition of a multilayer EUV reflection coating over the 2.65- $\mu\text{m}$  steps of such a high-pitch grating might result in non-negligible loss of EUV optical efficiency. (The multilayer stack would typically be around 400-nm thick.) An additional limitation of this approach is that only one wavelength could be focused back onto the plasma, due to chromatic dispersion in the diffracted beam.

### Spectral Filtering with a Phase-Fresnel Collector Mirror

An alternative spectral filtering mechanism illustrated in Figure 4 similarly directs IR radiation onto a circle or halo surrounding the IF aperture, but not via diffractive scattering. Instead, the collector mirror shape is designed to direct specularly-reflected light out of the aperture, and a phase-Fresnel grating directs the EUV radiation into the aperture. (The grating dimensions are too small to significantly affect the IR and most other OoB radiation.) This method achieves virtually complete elimination of OoB radiation from the far IR to the deep VUV with minimal impact on EUV collection efficiency.

The first detail view in Figure 4 illustrates the phase-Fresnel grating profile in cross section. The 1-mrad light cone from the plasma source is reflected into a 1-mrad, zero-order reflected light cone in OoB wavelengths, and a 1-mrad, first-order diffracted light cone in the EUV (13.5 nm). The angular separation between the two cone axes must be greater than 1 mrad to achieve spatial separation of the zero and first orders. The grating blaze angle is half the diffractive deviation angle at the 13.5 nm blaze wavelength; hence the blaze angle is at least 0.5

mrad. For near-normal incidence, phase matching between Fresnel facets is achieved when the grating depth is half the blaze wavelength, i.e., 6.75 nm. (This is comparable to the thickness of a single bilayer in a Mo/Si EUV multilayer mirror stack.) For off-normal incidence the depth is greater by a factor of the reciprocal cosine of the incidence angle but is less than 10 nm over the full mirror aperture. Thus, the maximum allowable grating period is approximately  $(10 \text{ nm})/0.0005 = 20 \mu\text{m}$ . A significantly smaller period (larger diffraction angle) may be required to accommodate tolerance factors or other design constraints. (This assumes that the grating is blazed for the first diffraction order. As discussed below, the period can be much larger if a higher order is used.)

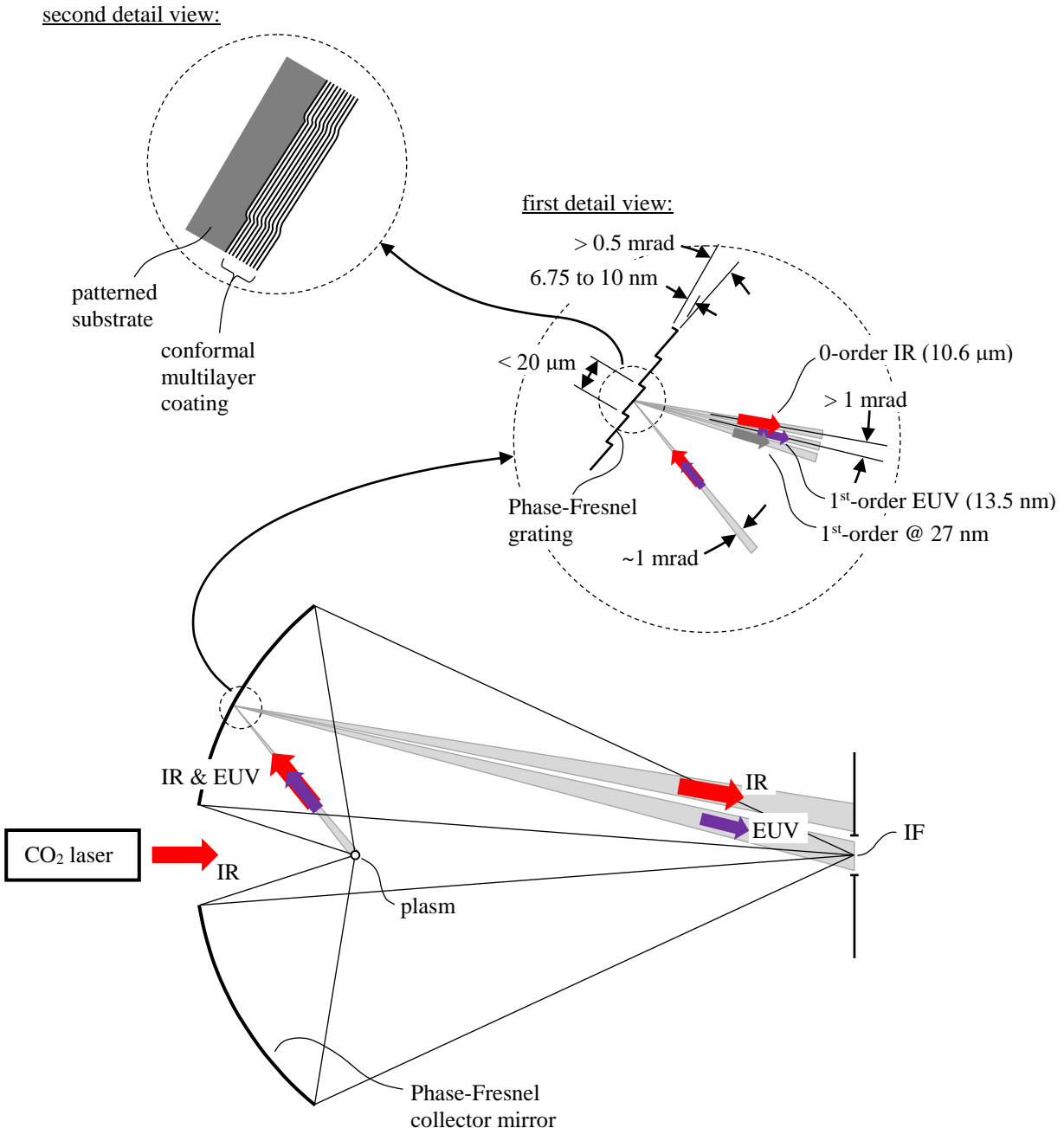


Figure 4. Phase-Fresnel-grating spectral filter.

The detail view in Figure 4 also illustrates a first-order diffraction cone for wavelength 27 nm (twice the 13.5-nm blaze wavelength), for which the diffraction angle is larger by a factor of 2 due to chromatic dispersion in the first order. This wavelength is angularly separated from the 13.5-nm EUV by at least 1 mrad and will hence be eliminated at the IF aperture. The diffraction angle is approximately proportional to wavelength; hence all wavelengths greater than twice the blaze wavelength will be eliminated.

The phase-Fresnel grating is patterned in a metal (e.g. nickel) substrate layer on the mirror, on which a multilayer EUV reflective coating (typically comprising Mo/Si bilayers) is conformally deposited, as illustrated in the second detail view in Figure 4. The performance capabilities of EUV phase-Fresnel gratings of this type are dramatically illustrated in Voronov et al. [Ref. 16], which demonstrates a blazed grating with profile depth 6.7 nm and a period of only 190 nm. The multilayer reflection coating (Mo/Si, 40 bilayers) has a thickness of 270 nm, which is larger than the period, but the grating exhibits EUV reflectance close to 40%. (See Figures 2 and 3 in Ref. 16.) A longer-period grating designed for second-order operation exhibits higher efficiency (52%). The grating structures used for the present application would have similar depth dimensions, but the minimum period would be up to two orders of magnitude larger than the Ref. 16 gratings. Thus, the EUV efficiency would not be expected to differ much from an unpatterned mirror, provided that the grating structure can be manufactured with adequately good surface finish.

Moriya et al. [Ref. 17] describe a spectral purity filter that is very similar to Figure 4, but in this system the grating structure is patterned in a multilayer film, not in the substrate. (See FIG. 3 in Ref. 17.) The layers are deposited on an unpatterned substrate, and the grating grooves are then cut into the multilayer stack. The grating profile would need to be very deep (e.g. about 250 times deeper than the 6.7-nm depth of the Figure-4 grating), and the structure would require very many Mo/Si bilayers (e.g., 300). The grating operates to concentrate OoB radiation in a first diffraction order, which is diverted out of the IF while EUV is substantially concentrated in the zero order. By contrast, the grating in Figure 4 operates to concentrate EUV into a first diffraction order while OoB radiation is either undeviated from the zero order or is scattered outside of the IF via chromatic dispersion.

The first-order diffraction efficiency  $\eta$  of the phase-Fresnel grating at wavelength  $\lambda$  is approximately

$$\eta = \text{sinc}^2[\pi(\lambda_B / \lambda - 1)]$$

where  $\lambda_B$  is the first-order blaze wavelength (13.5 nm) and  $\text{sinc}[x] = \frac{\sin x}{x}$ . ( $\text{sinc}[0] = 1$ .) This is the “relative efficiency”, normalized to the reflectance of an unpatterned mirror. (The formula is based on Fourier-optics approximations.) Within the 2% EUV wavelength band of an LPP source and collection mirror,  $\lambda$  is very close to  $\lambda_B$  and the above formula can be approximated as

$$\eta \approx 1 - \frac{1}{3}\pi^2 (\lambda_B / \lambda - 1)^2 \quad (\text{for } \lambda \approx \lambda_B).$$

The factor  $\lambda_b / \lambda$  is in the range 0.99 to 1.01 (for a lithography system with a 2% wavelength pass band), and  $\eta > 1 - 3.3 \times 10^{-4}$ , over the collected EUV spectrum. This implies that the grating's optical efficiency loss is negligible, but in practice there may be some non-negligible loss due to distortion of the multilayer EUV mirror coating by the step in the blaze profile.

The efficiency loss could possibly be mitigated by designing the grating to operate in a higher blaze order. For example, if the grating illustrated in Figure 4 is designed to operate in the second order, then the grating profile dimensions would be doubled (i.e., a depth in the range of 13.5 to 20 nm, period less than 40  $\mu\text{m}$ ) and the multilayer stack thickness would be a proportionately smaller fraction of the grating period. Also, a coarser grating structure might be more manufacturable. But there are two possible tradeoffs to using a higher blaze order: The rejection wavelength band is not as broad, and the grating's theoretical optical efficiency over the 2% EUV band will be somewhat reduced.

With second-order blazing, the Figure 4 illustration remains applicable with the grating dimensions doubled and the two "1<sup>st</sup>-order" labels replaced by "2<sup>nd</sup>-order". The second-order light cone at 27-nm wavelength is sufficiently separated from the second-order blaze wavelength, 13.5 nm. But the first order at 27 nm will be directly superimposed on the 13.5-nm second order; thus this wavelength will not be eliminated in the IF-filtered spectrum. However, the first-order light cone at 54 nm (4 times 13.5 nm) will coincide with the 27-nm second-order light cone, and this wavelength along with all higher wavelengths will be eliminated. In general, for a phase-Fresnel grating operating in the  $m$ -th diffraction order, the system will exclude all wavelengths greater than  $2m\lambda_b$ , where  $\lambda_b$  is the order- $m$  blaze wavelength (13.5 nm).

With order- $m$  blazing, the preceding efficiency formulas are modified as follows:

$$\eta = \text{sinc}^2[m\pi(\lambda_b / \lambda - 1)] \approx 1 - \frac{1}{3}m^2\pi^2(\lambda_b / \lambda - 1)^2$$

The optical loss is increased by approximately a factor of  $m^2$  relative to 1<sup>st</sup>-order blazing. For example, the loss at the 2% EUV band limits increases from  $3.3 \times 10^{-4}$  for first-order blazing to  $1.3 \times 10^{-3}$  with second-order blazing (a 4X increase). This is still insignificant, and optical efficiency would not be a limitation in using a higher blaze order. Even with 10<sup>th</sup>-order blazing the efficiency loss would be less than 4%. (A 10<sup>th</sup>-order grating would exclude wavelengths greater than 270 nm.)

In the Figure 4 system the OoB radiation might, to some extent, be scattered by aperture diffraction at the collector mirror even if it is not significantly influenced by grating diffraction. If aperture diffraction could result in significant OoB leakage into the IF aperture, then the diffraction tails can be mitigated by aperture apodization (either phase or amplitude apodization).

### Power Recycling

The spectral filtering system can be adapted for power recycling by constructing the IF aperture as a small, annular retroreflecting mirror ("retro mirror"), which returns the rejected OoB radiation to the plasma; see Figure 5. Also, large spherical-shell retro mirrors can be arrayed around the plasma to salvage the uncollected OoB radiation. The retro mirrors create a kind of optical "echo chamber", which has the effect of amplifying the IR drive laser.

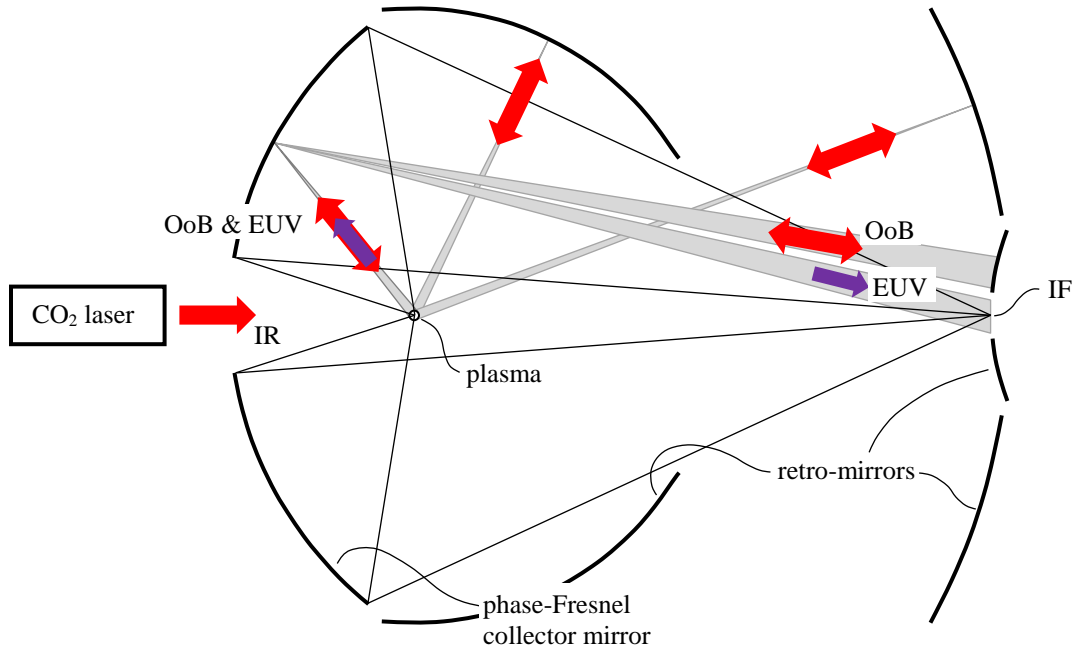


Figure 5. Power recycling.

A possible limitation of this system is that the retro mirrors will form an inverted image of the plasma onto itself. Only one plasma point at the design focus position will be accurately imaged onto itself, and any positional displacement of the plasma will cause its self-image to move in the opposite direction. Consequently, the power recycling efficiency would be sensitive to the plasma position, and statistical variations in the plasma location could result in EUV output power fluctuations. However, in the Figure-5 configuration the plasma is almost entirely surrounded by retroreflectors, so portions of the reflected radiation that do not intercept the plasma will be again retroreflected to form a twice-inverted plasma image, which will tend to track the plasma's positional variations and mitigate power fluctuations. (The two image inversions result in a non-inverted image.)

The mirrors can be designed to intentionally image the plasma to a separate conjugate focal point, which is axially displaced from the plasma, to ensure accurate and stable plasma self-imaging. For example, Figure 6 shows several illustrative OoB rays being reflected from the plasma center through the conjugate focal point, and then back to the plasma. This method can be termed “relay imaging”, in contrast to the “direct imaging” approach illustrated in Figure 5. The Addenda to this paper describe two other techniques for achieving erect (non-inverted) imaging of the plasma onto itself: a cat's-eye array (Addendum 1), and a corner-cube array (Addendum 2).

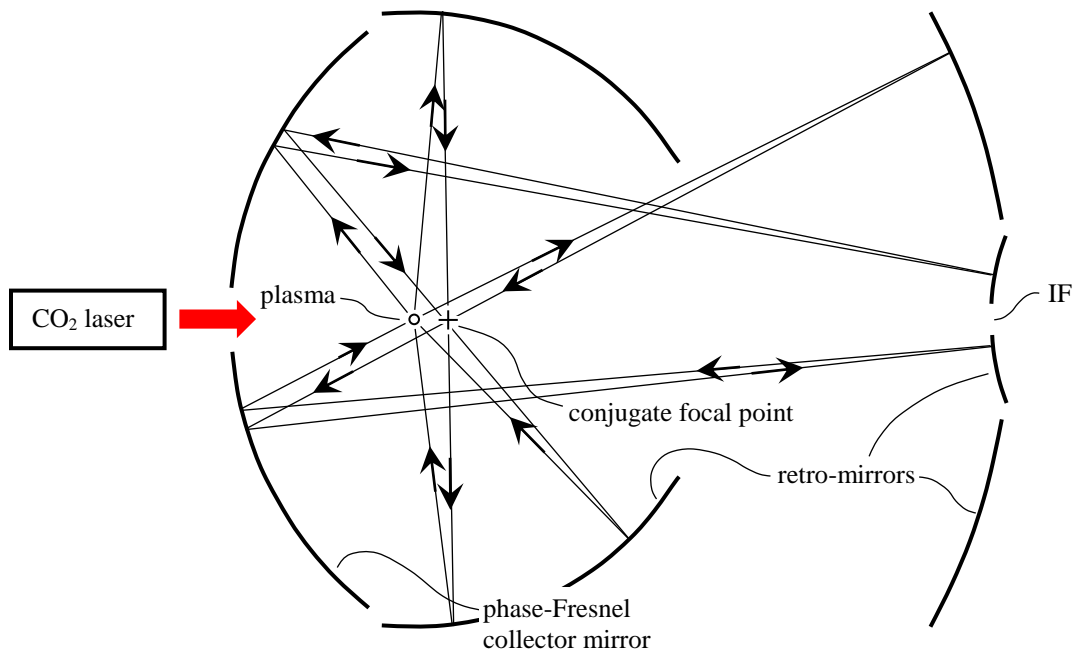


Figure 6. Power recycling with relay imaging.

There would be a slight time delay, on the order of 1 ns, between the plasma emission and reabsorption of recycled radiation due to the finite speed of light (300 mm/ns). Relay imaging would increase the delay relative to direct imaging, but the time would still be small in relation to the CO<sub>2</sub> laser pulse width, which is of order 20 ns FWHM. For some alternative LPP applications requiring a more compressed laser pulse the delay might be significant. The power recycling devices described in the Addenda may be preferred if the time delay needs to be minimized.

Power recycling would add some complication to the optical design because the collector's condenser mirror would need to operate in conjunction with the IF retro mirror as an OoB imaging device, which images the plasma back onto itself. One possible optical construction geometry is illustrated in Figure 7. (This configuration is designed for direct imaging but can be modified for relay imaging as shown in Figure 6.)

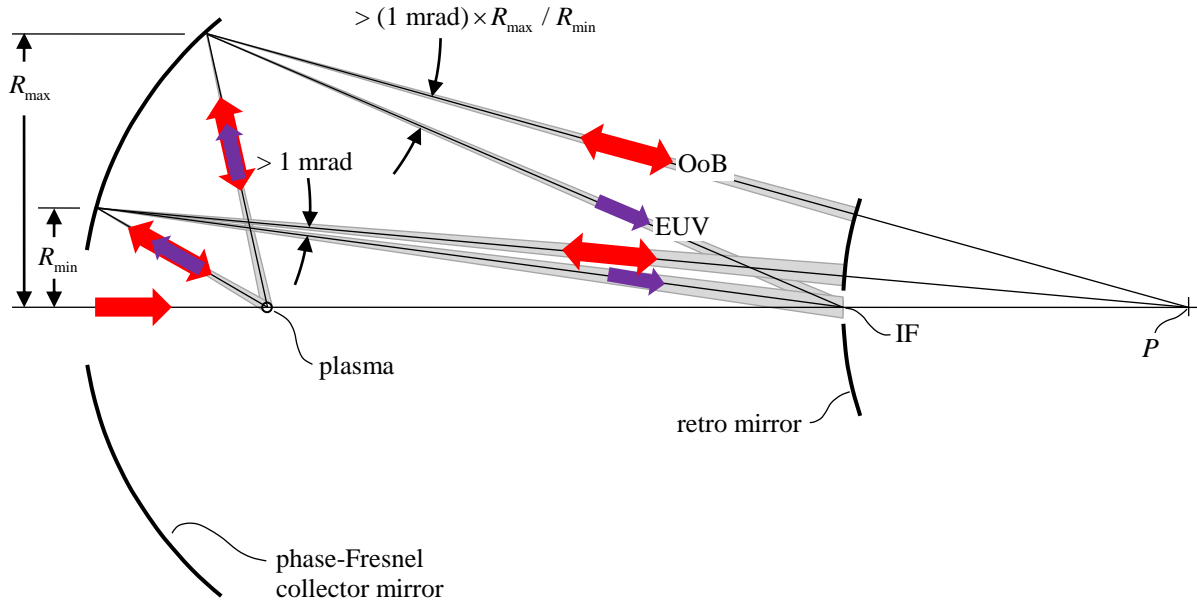


Figure 7 Collector geometry for power recycling.

The optics are designed to recycle OoB radiation intercepting the collector mirror between minimum and maximum aperture radii  $R_{\min}$  and  $R_{\max}$ , respectively. (These radii may or may not coincide with annular mirror aperture limits, but the mirror is only designed to recycle radiation within these limits.) The portion of the collector mirror within this radius range is ellipsoidal, and it images zero-order geometric rays from the plasma center onto a conjugate axial point  $P$  on the line through the plasma center and the IF. (Point  $P$  can be on either side of the IF.) The retro mirror is a spherical surface centered at  $P$ , and it has an annular aperture. EUV (13.5-nm) rays are diffractively focused to the axial IF point at the center of the annular aperture.

The specularly reflected OoB light cone and diffracted EUV light cone from an inner aperture point at radius  $R_{\min}$  must have an angular separation of at least 1 mrad between the cone axes, as described above, to avoid any overlap between the cones (Figure 7; cf. Figure 4). For other aperture points the angular separation is larger in approximate proportion to the point's radial distance from the optical axis. Thus, for an outer aperture point at radius  $R_{\max}$  the OoB and EUV ray separation angle is approximately  $(1 \text{ mrad}) \times R_{\max} / R_{\min}$  or greater. For example, with  $R_{\max} / R_{\min} = 5$  the separation angle would be at least 5 mrad, the grating blaze angle would be at least 2.5 mrad, and the grating period would be less than  $4 \mu\text{m}$  (for 1<sup>st</sup>-order blazing, or  $4m \mu\text{m}$  for order- $m$  blazing). In general, with power recycling the grating blaze angle and line density at the mirror periphery may need to increase by approximately a factor of  $R_{\max} / R_{\min}$  relative to what would be required to just separate the OoB and EUV.

It should be noted that even the  $4\text{-}\mu\text{m}$  grating period in the above example is more than an order of magnitude larger than the 190-nm period of the Ref. 16 grating. But if a longer grating

period would be preferred, then the power-recycling optics can be modified as illustrated in Figure 8. In this configuration some spherical aberration is designed into the focused zero-order beam to limit the OoB-EUV separation angle. Zero-order rays reflected from the collector mirror near the center (at radius  $R_{\min}$ ) intercept the optical axis at point  $P$ , as in Figure 7. But rays reflecting from the periphery (at radius  $R_{\max}$ ) cross the axis at point  $P'$ , closer to the  $IF$ . (Other rays cross the axis at intermediate points.) This reduces the angle between the reflected OoB and diffracted EUV rays, resulting in a lower grating line density. The tradeoff to this advantage is that the retroreflector will be smaller and will operate over a greater angular range, possibly resulting in greater imaging aberrations and compromised power recycling performance.

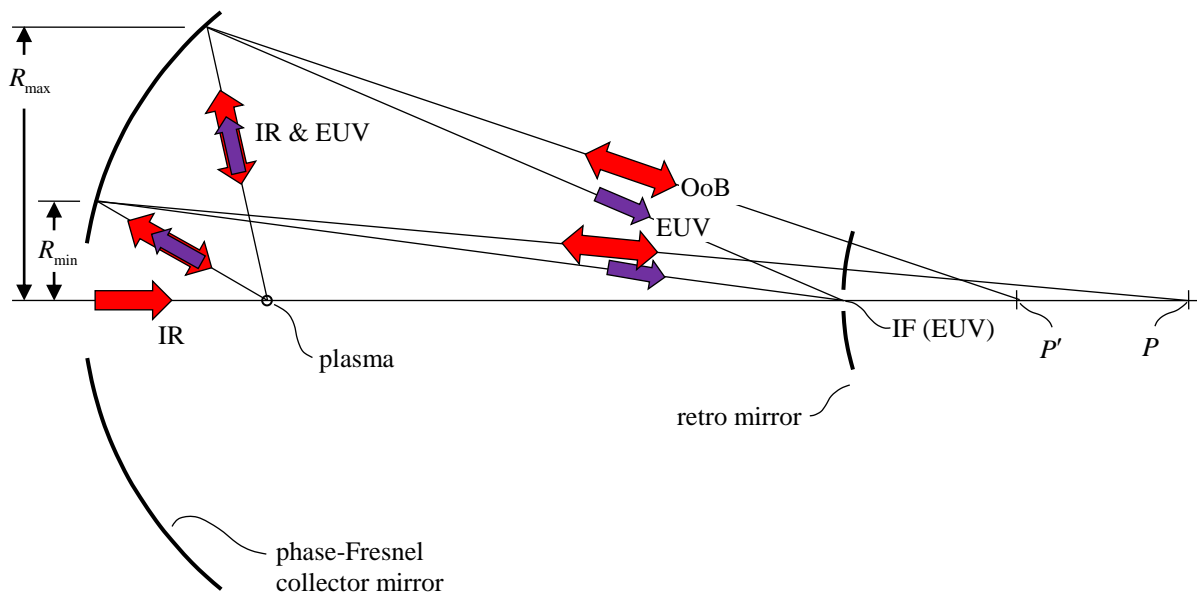


Figure 8. Spectral filter with spherically aberrated zero-order focus.

### Grating Manufacture

The phase-Fresnel grating can be fabricated by the method used by Kriese et al. [Ref. 7], i.e., single-point diamond turning on a nickel-plated substrate followed by application of a smoothing layer to remove the diamond machining marks. Feigl et al. [Ref. 8] formed complex grating structures by ion etching into a polished nickel mirror. Phase-Fresnel gratings could similarly be formed by an “ion turning” process analogous to diamond turning but using a focused ion beam in place of the diamond cutter. Moriya et al. [Ref. 17] describe a similar manufacturing process for patterning grating grooves in a multilayer film, and the same approach can be used for patterning a mirror substrate. (See FIG. 10 in Ref. 17.)

The linear-profile, sawtooth form of phase Fresnel facets can be approximated by a multi-level, stepped profile, which can be fabricated by ion-beam (or e-beam) patterning of a multilayer film with embedded etch stops. [Ref 18] The last patterning step selectively etches

the structure down to the etch-stop layers, so the grating profile can be controlled to atomic-scale depth dimensions if a deposition process such as magnetron sputtering or atomic layer deposition is used.

## Conclusion

Phase-Fresnel grating structures formed on EUV collector mirrors can be used to efficiently eliminate out-of-band LPP radiation over the full IR-to-VUV spectrum without significantly compromising EUV collection efficiency. The rejected or uncollected OoB power can potentially be recycled back to the plasma via retroreflection to improve EUV conversion efficiency.

## Addendum 1: Cat's-Eye Array

Figure 9 illustrates a variation of Figure 5 in which the spherical retro mirrors are double-shell reflectors, each comprising a transmitting inner shell and a reflecting outer shell. The enlarged detail view in Figure 9 shows a cross-sectional view of a double-shell reflector. An array of converging lenses on the inner shell images the plasma onto foci on the outer shell, and an array of concave mirrors on the outer shell retroreflects the plasma images back through the lenses. Each lens is paired with a corresponding mirror, and the two in combination operate as a cat's-eye retroreflector. Accurate retroreflection is maintained even as the plasma position varies (as indicated by the dashed ray lines and direction arrow in Figure 9). Thus, the alignment tolerance between each cat's eye reflector and the plasma would be non-critical.

The beam reflected from each cat's-eye element has a diffraction-limited angular spread of approximately  $\lambda / w$ , where  $\lambda$  is the wavelength and  $w$  is the lens aperture width. The diffractive spread should be smaller than the plasma subtend angle  $\delta$  at the reflector:  $\lambda / w < \delta$ .  $w$  would typically be significantly larger than 10 mm. At the 10.6- $\mu\text{m}$  IR wavelength, this results in a diffractive spread less than 1 mrad (i.e.,  $\lambda / w < 0.001$ ), which is comparable to  $\delta$  for typical LPP geometries.

A periodic array of cat's-eye reflectors generally operates as a diffraction grating that concentrates most of the reflected energy into multiple diffraction orders close to the geometric-optics reflected ray direction. The angular separation between diffraction orders is approximately  $\lambda / w$ , which should be small in relation to  $\delta$  to ensure that the reflected energy is concentrated onto the plasma. Thus, the condition  $\lambda / w < \delta$  holds irrespective of whether coherent interactions between cat's-eye elements are considered.

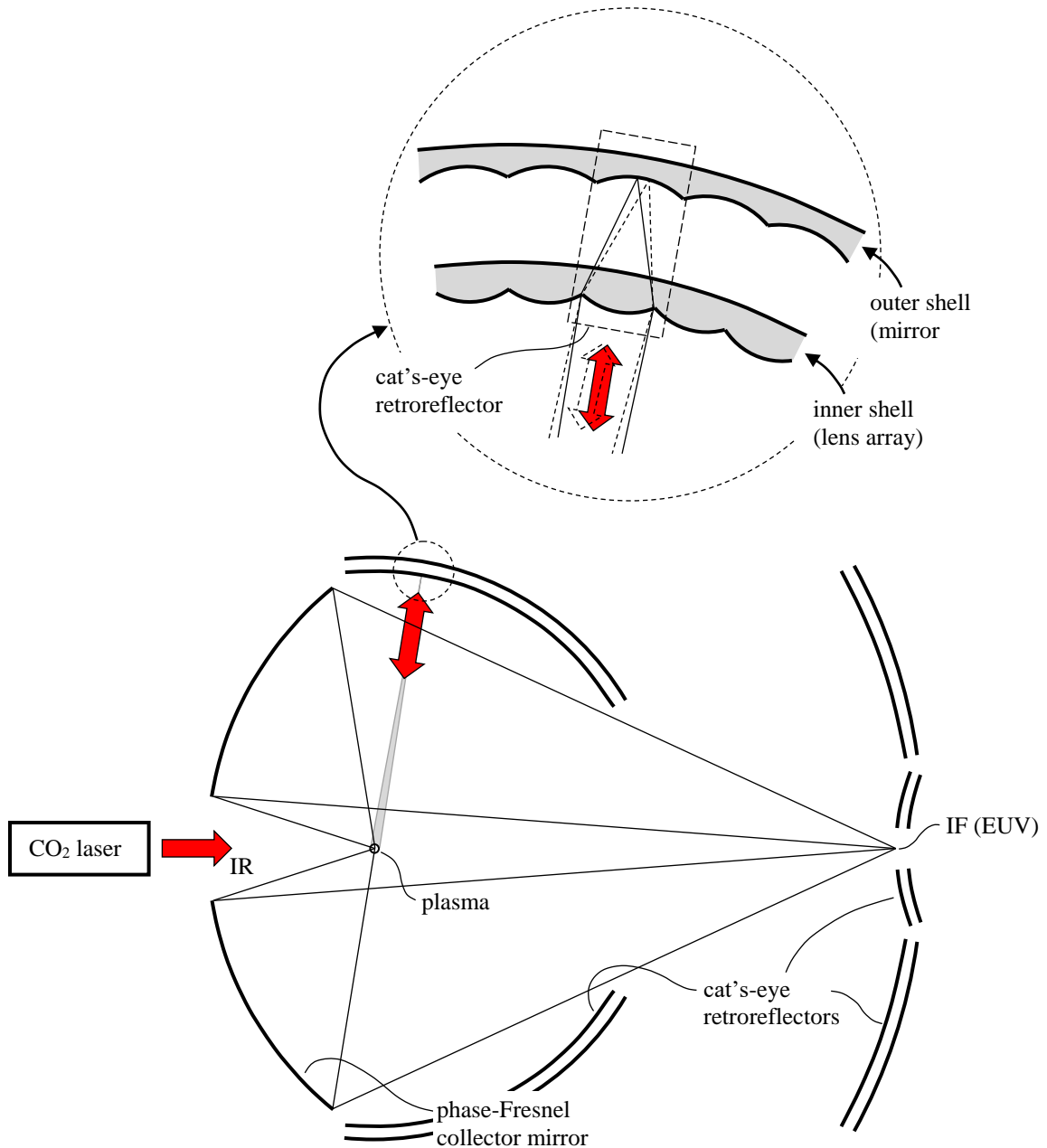


Figure 9. Power recycling with cat's-eye retroreflectors.

The Figure-9 configuration can be simplified in several ways. The space between the two shells could be filled with solid dielectric material, in which case the outer shell would simply be a reflective mirror coating formed on the inner shell's back side. The lenses and mirrors can be replaced by phase-Fresnel elements (e.g. using a lithographic patterning process). The spherical-shell substrates can be replaced by flat plates, using off-axis lenses or mirrors to accommodate off-axis illumination on the plates' peripheral region. For example, Figure 10 shows a cross-sectional view of a flat-plate design using phase-Fresnel lenses and off-axis, phase-Fresnel mirrors.

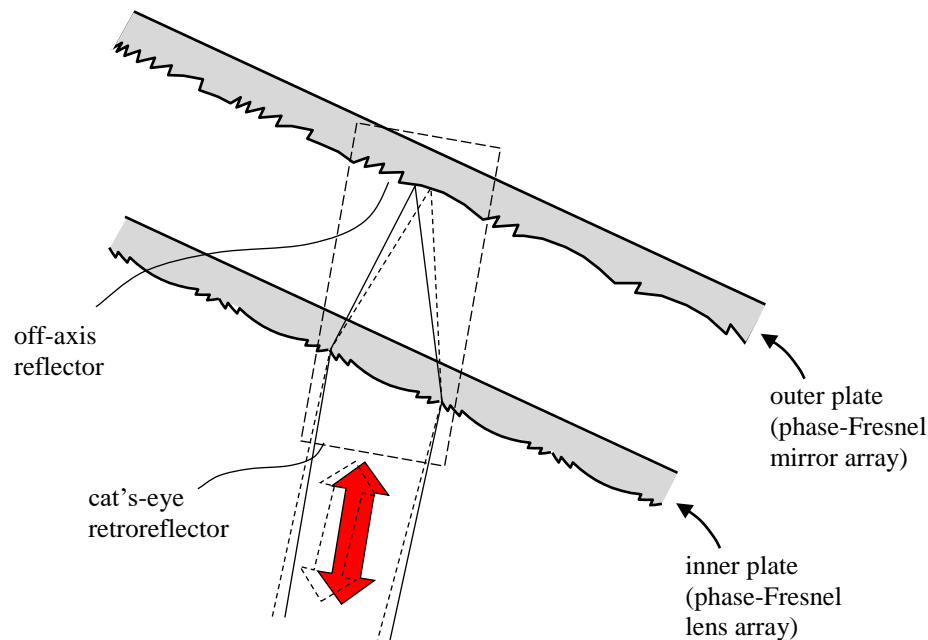


Figure 10. Flat-plate cat's-eye retroreflector design with phase-Fresnel optics.

The retroreflector mirror elements need not necessarily be curved. Figure 11 illustrates a flat-plate design using off-axis lenses and a flat mirror surface. Each lens focuses the plasma's center point into a convergent light cone with the cone axis normal to the mirror. There may be some slight vignetting of the reflected light cone by the lens aperture when the plasma position changes, but accurate plasma self-imaging will still be maintained.

The cat's-eye array elements need not be contiguous; they could be discrete components as illustrated in Figure 12. In this illustration, each cat's-eye element is a solid glass element with an on-axis, convex lens surface and a flat, reflective back surface. The lens axes are aligned to the plasma center, but the alignment tolerance is much looser than the plasma subtend angle. In a variation of this configuration, each cat's-eye unit could be a miniature lens system that is optimized for wide-field imaging performance.

The solid angular range around the plasma can be efficiently partitioned between individual cat's-eye reflectors by using a Goldberg polyhedron [Ref. 19] as an aperture patterning template. An example of a Goldberg polyhedron is illustrated in Figure 13. Each cat's-eye aperture would be delimited by the solid angular range defined by one of the polyhedron faces.

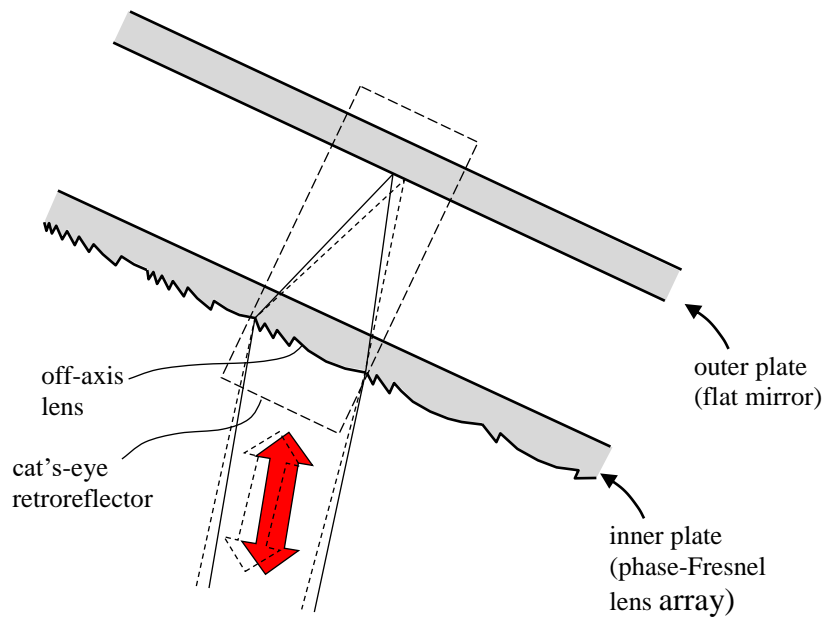


Figure 11. Cat's-eye retroreflector array with flat mirror.

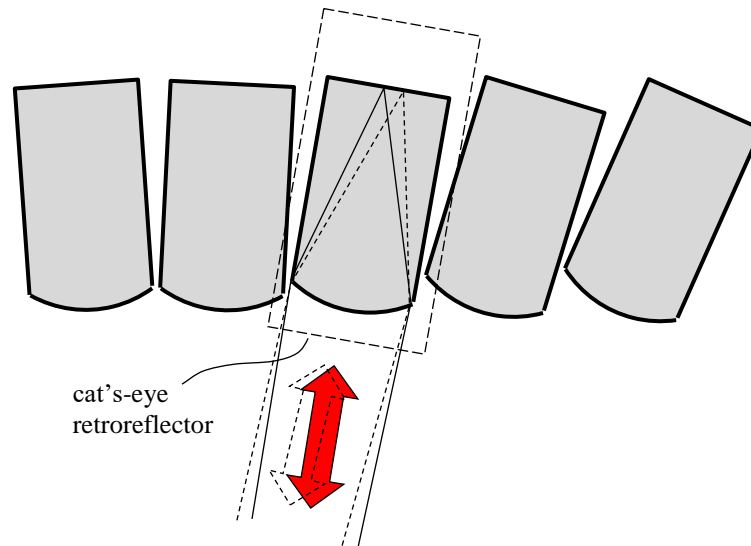


Figure 12. Discontiguous cat's-eye array.

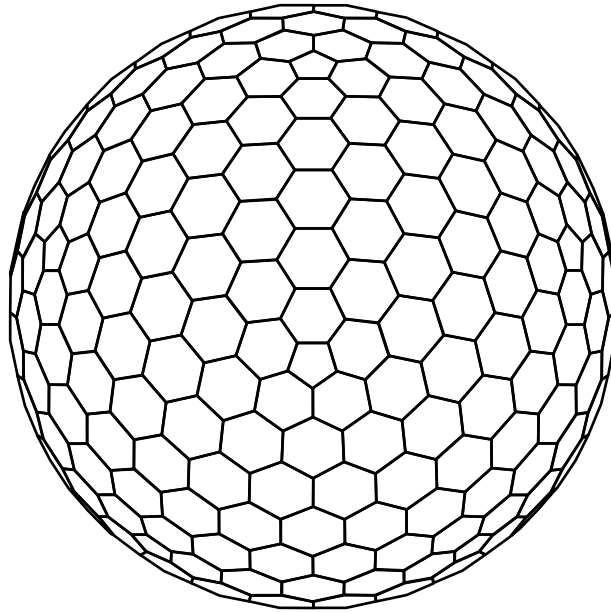


Figure 13. Goldberg polyhedron

A cat's-eye array can efficiently retroreflect the 10.6- $\mu\text{m}$  IR radiation to the plasma but may not be able to retroreflect much of the other OoB radiation due to chromatic dispersion in the lens. The system could use a hybrid diffractive/refractive lens design (similar to a phase-Fresnel lens, but on a curved substrate), although this would only allow accurate point imaging at two wavelengths and could not operate efficiently over a very wide spectral range. Also, infrared lens materials (e.g. zinc selenide, ZnSe, for 10.6- $\mu\text{m}$  IR) have transmittance limits at shorter wavelengths. These limitations can be overcome by using parabolic-mirror focusing elements instead of lenses, or by using corner-cube reflectors as described in Addendum 2.

#### Addendum 2: Corner-Cube Reflector Array

Figure 14 shows another variation of Figure 5 in which the spherical retro mirrors comprise corner-cube retroreflector arrays. The mirrors are illustrated schematically by a sawtooth profile, but each retroreflector is a three-surface, corner-cube element.

Figure 15 illustrates a portion of a conventional corner-cube array, one element of which is shaded. From this perspective the incident beam reflects off the top of the array. Each corner cube's three reflective surfaces are planar, square, and mutually orthogonal, and the cube's aperture projection in the incidence direction is a regular hexagon. The device operates to retroreflect a collimated beam directed approximately parallel to an optical axis, which is oriented at the same angle (approximately  $54.7^\circ$ ) to all three reflector surface normals. The hexagonal aperture geometry can retroreflect rays that are parallel to the axis without geometric efficiency loss, although alternative aperture forms could also be used with only minor efficiency loss.

A conventional corner-cube design can be modified to achieve accurate self-imaging of an axial point at finite conjugate by making the reflector surfaces slightly concave, as described

in Ref. 20 (e.g. see Figure 4 in Ref. 20). The surface geometry has sufficient degrees of freedom to achieve perfect geometric self-imaging of the plasma center point (although the optimal surface shape might not be exactly spherical as described in Ref. 20). Off-axis aberrations would be insignificant in comparison to the plasma size, provided that the reflector elements are sufficiently small. (As with the cat's-eye array, the corner-cube aperture size may need to be significantly larger than 10 mm to avoid excessive image degradation from aperture diffraction. But with typical LPP dimensional scales, the corner cubes would nevertheless be small enough to limit off-axis geometric aberrations.)

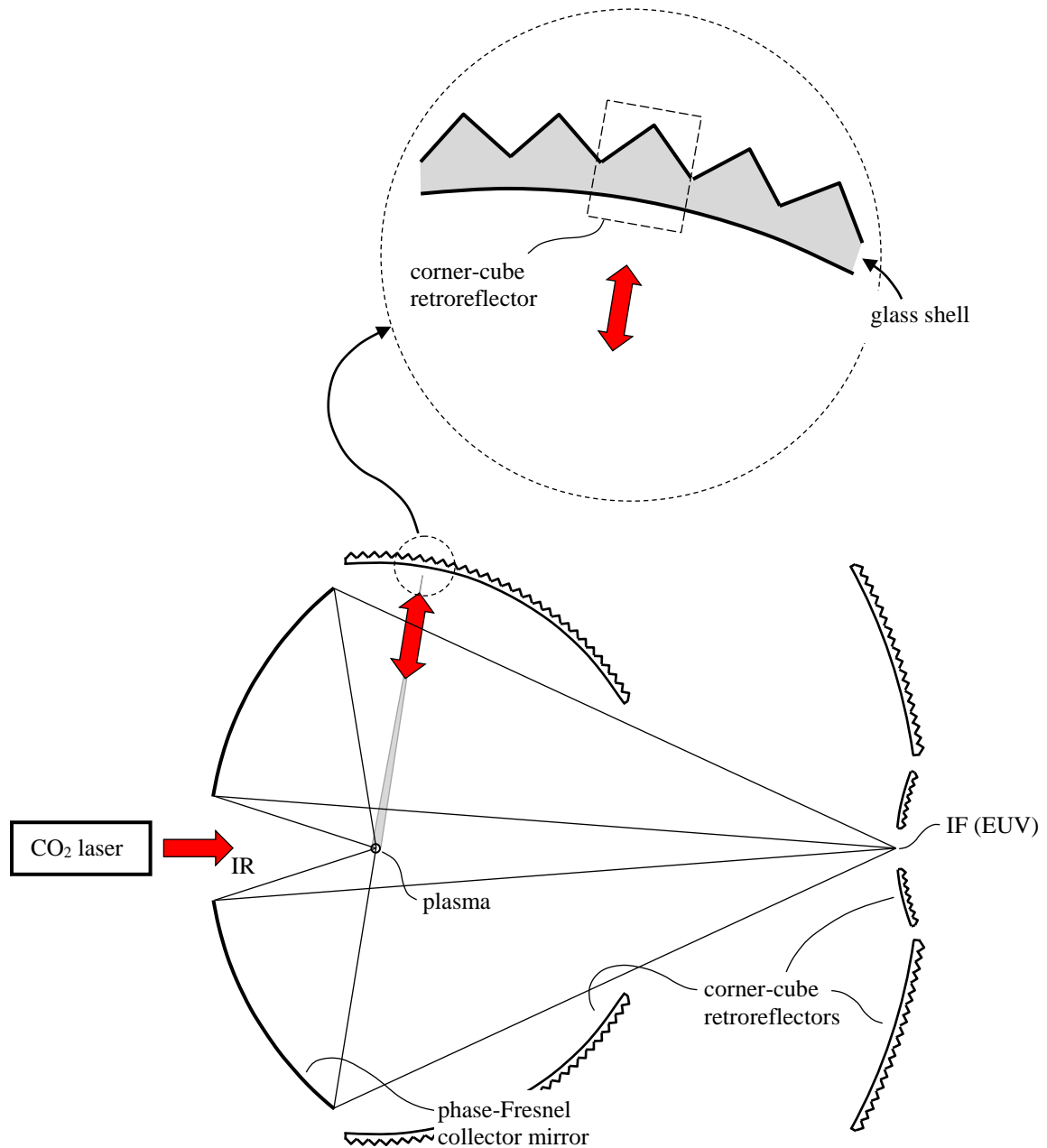


Figure 14. Power recycling with corner-cube retroreflectors.

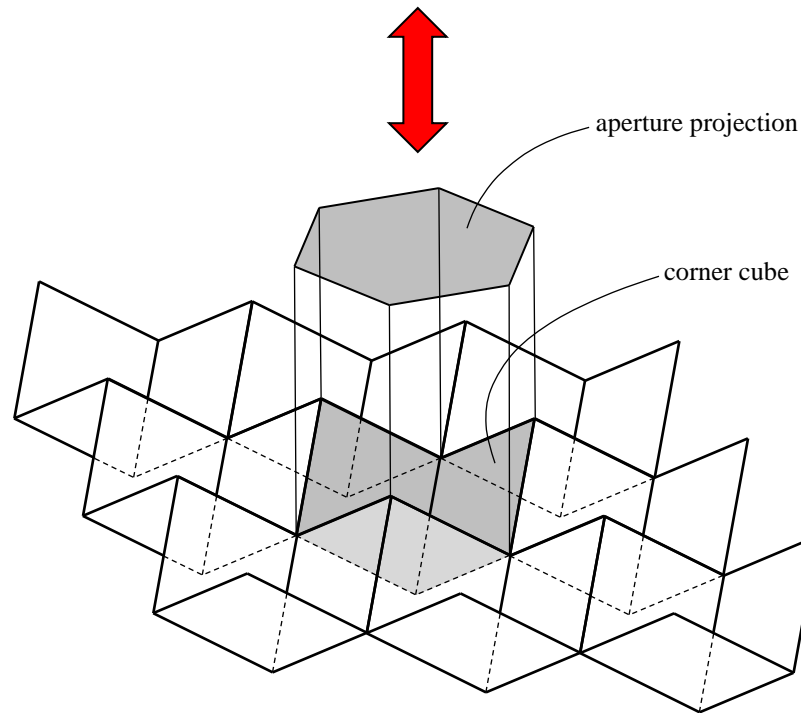


Figure 15. Corner-cube retroreflector array.

The enlarged detail view in Figure 14 schematically illustrates a cross-section of a corner-cube array formed in a solid glass shell with the reflectors formed on its back side. This type of device requires no reflective mirror coating; it can operate via total internal reflection. However, it could only retroreflect OoB radiation within a limited wavelength band because of the spectral transmittance limitations of common optical materials such as ZnSe. Alternatively, front-surface reflectors could be formed as recessed, pyramidal cavities with metal or dielectric-coated reflector surfaces. This avoids bulk transmittance losses in glass, although the spectral reflectance of common reflective coatings could be a limitation.

Figure 16 schematically illustrates an alternative to the Figure-14 configuration, using conventional, flat-face corner cubes. Collimating lenses (e.g. phase-Fresnel elements) on the reflector shell's inner surface collimate rays from the plasma center point, and these rays are retroreflected by the corner-cubes. If front-surface reflectors are used, then the collimating lenses can be formed on a separate, inner shell. (An advantage of this design over the Figure-9 double-shell configuration is that the shells need not be widely separated to accommodate the lens focal lengths. Chromatic dispersion would probably be insignificant because the collimating lenses have very low optical power.)

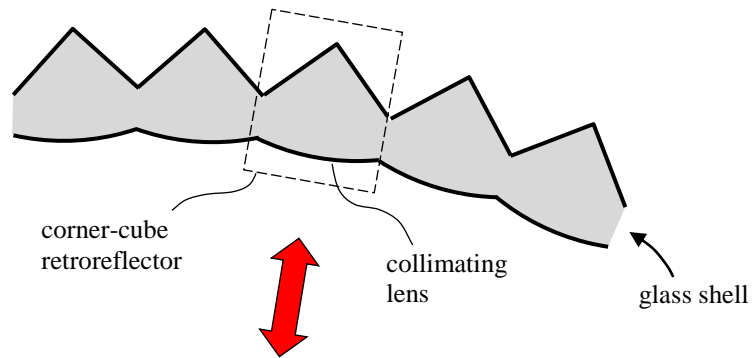


Figure 16. Flat-face corner-cube retroreflectors with collimating lenses.

The corner-cube arrays can be formed in a flat-plate configuration analogous to the flat-plate cat's-eye design of Figure 10. In this case the corner-cube optical axes would be tilted relative to the plate normal over the peripheral portions of the plate to accommodate the incident beam divergence, as illustrated in Figure 17. Alternatively, off-axis collimating lenses can be used to collimate the beams in a common direction, allowing the use of a uniformly periodic array of flat-face corner cube reflectors; see Figure 18.

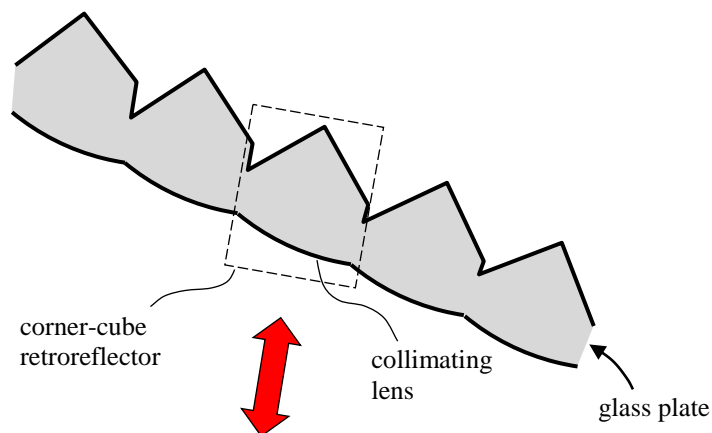


Figure 17. Flat-plate corner-cube array with tilted corner-cubes.

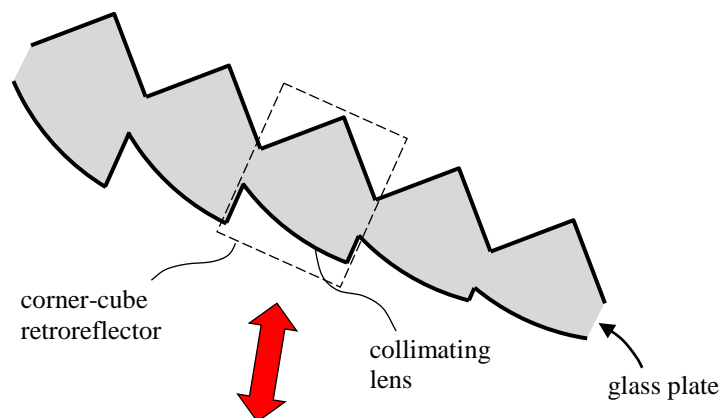


Figure 18. Flat-plate corner-cube array with off-axis collimating lenses.

A corner-cube reflector array can be fabricated by tiling an array of hexagonal-section bar segments, each of which has three precision-machined and polished corner-cube reflector surfaces on its end. The bar segments can be fused or bonded to a common substrate or can be used as a replication master for manufacturing the reflector array (e.g. by molding or electroplating).

The array can also be formed as a collection of discrete, non-contiguous corner-cube elements, as illustrated schematically in Figure 19. In this configuration the corner-cube elements are front-surface reflectors with slightly curved surfaces similar to the design described in Ref. 20. Alternatively, either flat-face or curved-face corner cubes could be preceded by miniature lenses or lens systems to achieve good wide-field imaging performance. The aperture partitioning can be based on a Goldberg polyhedron similar to that illustrated in Figure 13. All but 12 of the polyhedron faces are hexagonal (the exceptions being pentagons). The hexagons are not generally regular (i.e. equilateral and equiangular), but the irregularity is not significant.

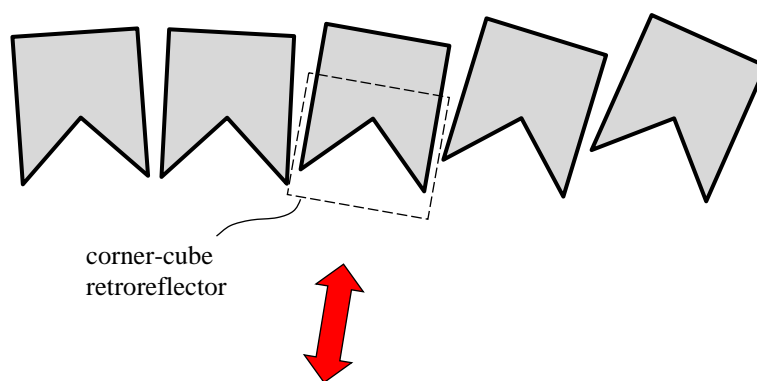


Figure 19. Discontinuous corner-cube array.

Figure 20 schematically illustrates another variation of the Figure 5 and Figure 14 configurations in which the collector focuses the reflected (zero-order) OoB radiation to a ring focus on a small axicon mirror, which reflects the focused radiation toward a larger corner-cube

retroreflector array. (In the illustrated configuration the zero-order beam crosses the collector's optical axis.) The corner cubes are constructed to retroreflect a geometric wavefront from the plasma center back to the ring focus, and the axicon reflects the radiation back to the collector and onto the plasma.

The axicon is a conical (or approximately conical) mirror, which could be an actively-cooled molybdenum mirror that can withstand high radiation levels. This design allows the angular offset between the OoB and EUV beams to be fairly small (e.g., not much more than 1 mrad), resulting in a relatively long grating period (e.g., not much less than 10 micron). The long period is advantageous in terms of manufacturability, minimizing EUV efficiency loss, and minimizing chromatic dispersion within the 2% EUV collection band.

The corner cubes could be front-surface aluminum mirrors with a protective coating such as magnesium fluorid (MgF<sub>2</sub>) or lithium fluoride (LiF). Aluminum mirrors can exhibit good reflection efficiency from the vacuum ultraviolet to long-wave infrared [Ref. 21]. (The collector and the molybdenum axicon would exhibit high reflection efficiency at 10.6 micron, although their efficiency at short wavelengths would not be nearly as good as aluminum.)

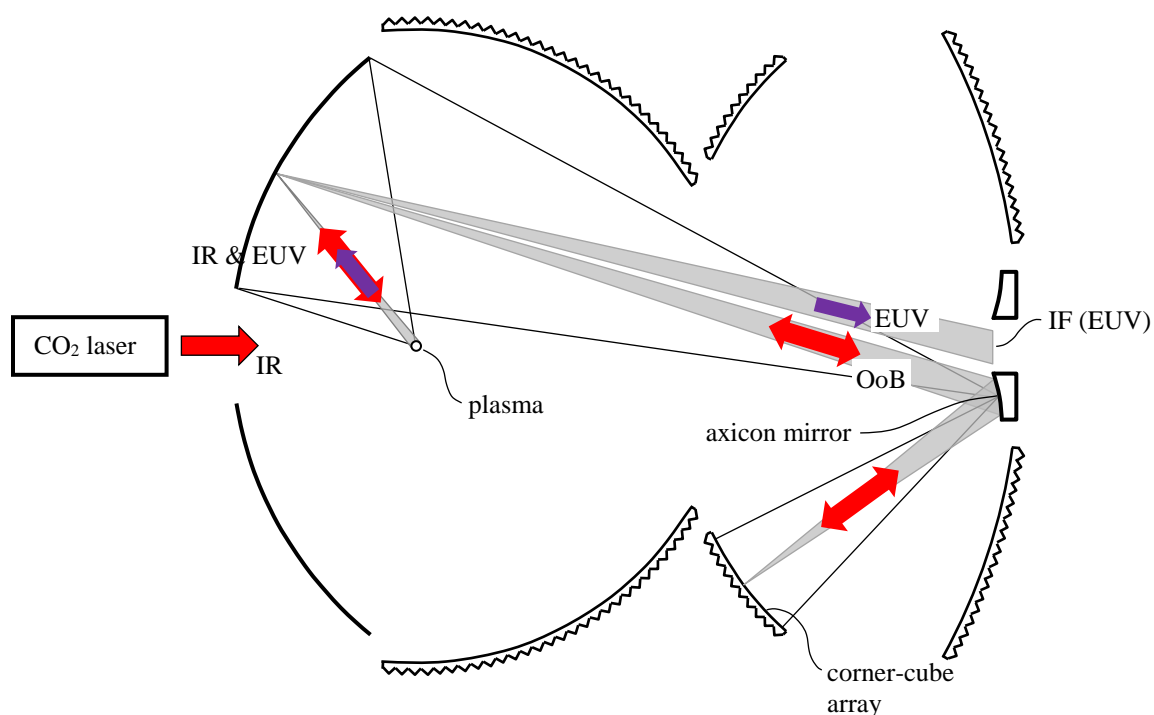


Figure 20. Power recycling from collector with axicon at ring focus.

MgF<sub>2</sub>-coated aluminum reflects efficiently down to wavelength 115 nm, and LiF-coated aluminum reflects down to 105 nm. (LiF is hygroscopic but can be protected with several nanometers of ALD AlF<sub>3</sub>.) [Ref's. 22, 23; also see Ref. 24] The high-efficiency range can be further extended down to about 60 nm by using bare aluminum. For example, Figure 21 illustrates the calculated compound reflectance of a corner-cube reflector (3 surface reflections at 54.7° incidence) for an uncoated aluminum front surface and a coated surface with 15 nm of

either  $\text{MgF}_2$  or  $\text{LiF}$ . Uncoated aluminum mirrors have been proposed for space-based telescopes [Ref. 25]. For application in an EUV plasma chamber, the mirror surface would need to be environmentally isolated by a pellicle cover, as illustrated schematically in Figure 22. Pellicle technology has been developed to an advanced stage for EUV photomasks [Ref's. 26, 27], although the design requirements would be somewhat different for a corner-cube enclosure. The pellicle would need to withstand the harsher environment of the plasma chamber but would not need to extend over a large photomask area and would not need to transmit wavelengths below 50 nm. Also, image quality is not critical so a very thin pellicle could be supported by, e.g., a thin-walled honeycomb structure.

The “bare Al” plot in Figure 21 does not take into account the pellicle transmittance loss, but a pellicle such as monolayer graphene would exhibit over 90% transmittance efficiency (single-pass) from the near IR down to at least 200 nm. See Fig. 5 in Ref. 28. The figure does not go below 200 nm but it shows an absorption peak at 258 nm (4.8 eV), and transmittance might also be limited by absorption peaks at 194 nm (6.4 eV) and probably 146 nm (8.5 eV).

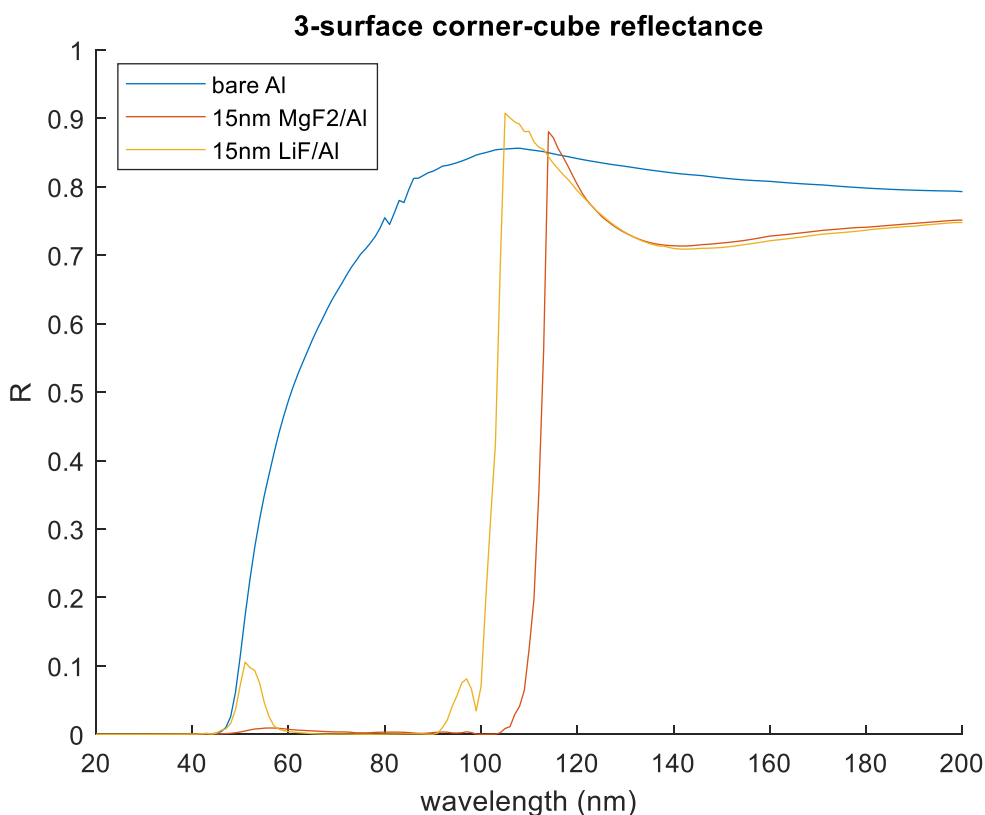


Figure 21. Corner-cube compound reflectance with bare or coated front-surface mirrors.

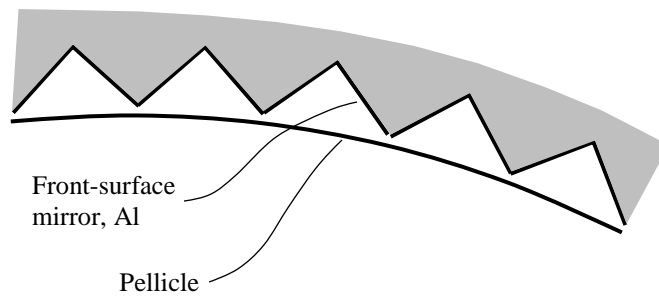


Figure 22. Bare-aluminum corner-cube reflector with pellicle.

LiF could also be used for corner-cube prism reflectors using total internal reflection. But in addition to the energy loss below wavelength 105 nm, there would also be significant loss in the range 105-125 nm for optical path lengths of order 1 cm through bulk LiF. Furthermore, there would be significant surface reflectance losses, although these could be mitigated by using “moth eye” antireflection surfaces.

## References

1. Miyamoto, Kenro. "The phase Fresnel lens." *JOSA* 51, no. 1 (1961): 17-20.  
<http://dx.doi.org/10.1364/JOSA.51.000017>
2. Park, Chang-Min, Insung Kim, Sang-Hyun Kim, Dong-Wan Kim, Myung-Soo Hwang, Soon-Nam Kang, Cheolhong Park, Hyun-Woo Kim, Jeong-Ho Yeo, and Seong-Sue Kim. "Prospects of DUV OoB suppression techniques in EUV lithography." In *SPIE Advanced Lithography*, pp. 90480S-90480S. International Society for Optics and Photonics, 2014.  
<http://dx.doi.org/10.1117/12.2046132>
3. Huang, Qiushi, Meint de Boer, Jonathan Barreux, Daniel M. Paardekooper, Toine van den Boogaard, Robbert van de Kruijs, Erwin Zoethout, Eric Louis, and Fred Bijkerk. "Spectral purity enhancement for the EUV lithography systems by suppressing UV reflection from multilayers." In *SPIE Advanced Lithography*, pp. 90480G-90480G. International Society for Optics and Photonics, 2014.  
<http://dx.doi.org/10.1117/12.2046415>
4. van den Boogaard, A. J. R., F. A. van Goor, E. Louis, and F. Bijkerk. "[Wavelength separation from extreme ultraviolet mirrors using phaseshift reflection.](#)" *Optics letters* 37, no. 2 (2012): 160-162.  
<http://dx.doi.org/10.1364/OL.37.000160>
5. Medvedev, V. V., A. J. R. van den Boogaard, R. van der Meer, A. E. Yakshin, E. Louis, V. M. Krivtsun, and F. Bijkerk. "[Infrared diffractive filtering for extreme ultraviolet multilayer Bragg reflectors.](#)" *Optics express* 21, no. 14 (2013): 16964-16974.  
<http://dx.doi.org/10.1364/OE.21.016964>
6. Trost, Marcus, Sven Schröder, Angela Duparré, Stefan Risse, Torsten Feigl, Uwe D. Zeitner, and Andreas Tünnermann. "[Structured Mo/Si multilayers for IR-suppression in laser-produced EUV light sources.](#)" *Optics express* 21, no. 23 (2013): 27852-27864.  
<http://dx.doi.org/10.1364/OE.21.027852>
7. Kriese, Michael, Yuriy Platonov, Bodo Ehlers, Licai Jiang, Jim Rodriguez, Ulrich Mueller, Jay Daniel et al. "Development of an EUVL collector with infrared radiation suppression." In *SPIE Advanced Lithography*, pp. 90483C-90483C. International Society for Optics and Photonics, 2014.  
<http://dx.doi.org/10.1117/12.2049279>
8. Feigl, Torsten, Marco Perske, Hagen Pauer, Tobias Fiedler, Uwe Zeitner, Robert Leitel, Hans-Christoph Eckstein et al. "Sub-aperture EUV collector with dual-wavelength spectral purity filter." In *SPIE Advanced Lithography*, pp. 94220E-94220E. International Society for Optics and Photonics, 2015.  
<http://dx.doi.org/10.1117/12.2175666>

9. Bayraktar, Muharrem, Fred A. van Goor, Klaus J. Boller, and Fred Bijkerk. "[Spectral purification and infrared light recycling in extreme ultraviolet lithography sources.](#)" *Optics express* 22, no. 7 (2014): 8633-8639.  
<http://dx.doi.org/10.1364/OE.22.008633>
10. Kierey, Holger, Klaus F. Heidemann, Bernd H. Kleemann, Renate Winters, Wilhelm J. Egle, Wolfgang Singer, Frank Melzer, Rutger Wevers, and Martin Antoni. "[EUV spectral purity filter: optical and mechanical design, grating fabrication, and testing.](#)" In *Optical Science and Technology, SPIE's 48th Annual Meeting*, pp. 70-78. International Society for Optics and Photonics, 2004.  
<http://dx.doi.org/10.1117/12.507741>
11. Liddle, J. Alexander, Farhad Salmassi, Patrick P. Naulleau, and Eric M. Gullikson. "[Nanoscale topography control for the fabrication of advanced diffractive optics.](#)" *Journal of Vacuum Science & Technology B* 21, no. 6 (2003): 2980-2984.  
<http://dx.doi.org/10.1116/1.1622938>
12. Van den Boogaard, A. J. R., E. Louis, F. A. Van Goor, and Fred Bijkerk. "[Optical element for full spectral purity from IR-generated EUV light sources.](#)" In *SPIE Advanced Lithography*, pp. 72713B-72713B. International Society for Optics and Photonics, 2009.  
<http://dx.doi.org/10.1117/12.829011>
13. Chkhalo, Nikolay I., Mikhail N. Drozdov, Evgeny B. Kluev, Aleksei Ya Lopatin, Valerii I. Luchin, Nikolay N. Salashchenko, Nikolay N. Tsybin, Leonid A. Sijmaenok, Vadim E. Banine, and Andrei M. Yakunin. "Free-standing spectral purity filters for extreme ultraviolet lithography." *Journal of Micro/Nanolithography, MEMS, and MOEMS* 11, no. 2 (2012): 021115-1.  
<http://dx.doi.org/10.1117/1.JMM.11.2.021115>
14. Suzuki, Yukio, Kentaro Totsu, Masaaki Moriyama, Masayoshi Esashi, and Shuji Tanaka. "Free-standing subwavelength grid infrared cut filter of 90mm diameter for LPP EUV light source." *Sensors and Actuators A: Physical* (2014).  
<http://dx.doi.org/10.1016/j.sna.2014.07.006>
15. Medvedev, V. V., A. E. Yakshin, R. W. E. van de Kruijs, V. M. Krivtsun, A. M. Yakunin, K. N. Koshelev, and F. Bijkerk. "Infrared antireflective filtering for extreme ultraviolet multilayer Bragg reflectors." *Optics Letters* 37, no. 7 (2012): 1169-1171.  
<http://dx.doi.org/10.1364/OL.37.001169>
16. Voronov, D. L., E. M. Gullikson, F. Salmassi, T. Warwick, and H. A. Padmore. "Enhancement of diffraction efficiency via higher-order operation of a multilayer blazed grating." *Optics Letters* 39, no. 11 (2014): 3157-3160.  
<http://dx.doi.org/10.1364/OL.39.003157>

17. Moriya, Masato, Osamu Wakabayashi, and Georg Soumagne. "Mirror for extreme ultra violet, manufacturing method for mirror for extreme ultra violet, and far ultraviolet light source device." U.S. Patent 8,592,787, issued November 26, 2013.  
<http://www.pat2pdf.org/patents/pat8592787.pdf>
18. Smith, Donald L., James C. Mikkelsen Jr, Babur B. Hadimioglu, and Martin G. Lim. "Method for fabrication of multi-step structures using embedded etch stop layers." U.S. Patent 6,187,211, issued February 13, 2001.  
<http://www.pat2pdf.org/patents/pat6187211.pdf>
19. Wikipedia, "Goldberg polyhedron".  
[https://en.wikipedia.org/wiki/Goldberg\\_polyhedron](https://en.wikipedia.org/wiki/Goldberg_polyhedron)
20. Macken, John. "Corner cube utilizing generally spherical surfaces." U.S. Patent 4,941,731, issued July 17, 1990.  
<http://www.pat2pdf.org/patents/pat4941731.pdf>
21. Wilbrandt, Steffen, Olaf Stenzel, Hiroshi Nakamura, D. Wulff-Molder, A. Duparré, and N. Kaiser. "Protected and enhanced aluminum mirrors for the VUV." *Applied Optics* 53, no. 4 (2014): A125-A130.  
<https://doi.org/10.1364/AO.53.00A125>
22. John J. Hennessy, Kunjithapatham Balasubramanian, Christopher S. Moore, April D. Jewell, Shouleh Nikzad, Kevin C. France, Manuel A. Quijada, "Performance and prospects of far ultraviolet aluminum mirrors protected by atomic layer deposition," *Journal of Astronomical Telescopes, Instruments, and Systems* 2(4), 041206 (7 June 2016).  
<https://doi.org/10.1117/1.JATIS.2.4.041206>
23. Brian Fleming, Manuel Quijada, John Hennessy, Arika Egan, Javier Del Hoyo, Brian A. Hicks, James Wiley, Nicholas Kruczek, Nicholas Erickson, and Kevin France, "Advanced environmentally resistant lithium fluoride mirror coatings for the next generation of broadband space observatories," *Appl. Opt.* 56, 9941-9950 (2017)  
<https://arxiv.org/abs/1801.03102>
24. NASA Technology Transfer Program, GSC-TOPS-94.  
<https://technology.grc.nasa.gov/patent/GSC-TOPS-94>
25. David D. Allred, R. Steven Turley, Stephanie M. Thomas, Spencer G. Willett, Michael J. Greenburg, Spencer B. Perry, "Adding EUV reflectance to aluminum-coated mirrors for space-based observation", *Proc. SPIE* 10398, UV/Optical/IR Space Telescopes and Instruments: Innovative Technologies and Concepts VIII, 103980Y (5 September 2017).  
<https://doi.org/10.1117/12.2274694>
26. Sung-Gyu Lee, Guk-Jin Kim, Su-Mi Hur, Hye-Keun Oh, "Search for multi-stack EUV pellicle membrane for EUV non-actinic mask inspection", *Proc. SPIE* 10450, International Conference on Extreme Ultraviolet Lithography 2017, 104501M (16 October 2017).  
<http://vixra.org/abs/1512.0295>

<https://doi.org/10.1117/12.2280618>

27. Marina Y. Timmermans, Ivan Pollentier, Jae Uk Lee, Johan Meersschaut, Olivier Richard, Christoph Adelman, Cedric Huyghebaert, Emily E. Gallagher, “CNT EUV pellicle: moving towards a full-size solution”, *Proc. SPIE* 10451, Photomask Technology, 104510P (16 October 2017).

<https://doi.org/10.1117/12.2280632>

28. Baokun Song, Honggang Gu, Simin Zhu, Hao Jiang, Xiuguo Chen, Chuanwei Zhang, Shiyuan Liu, “Broadband optical properties of graphene and HOPG investigated by spectroscopic Mueller matrix ellipsometry”, *Applied Surface Science* 439, 1079-1087 (2018).

<https://doi.org/10.1016/j.apsusc.2018.01.051>

<http://vixra.org/abs/1512.0295>